Desalination and Water Treatment
www.deswater.com

doi: 10.1080/19443994.2015.1094675

57 (2016) 18109–18119
August

Taylor & Francis
Taylor & Francis Group

CFD simulation of heat and mass transport for water transfer through hydrophilic membrane in direct-contact membrane distillation process

Mohsen Hasanizadeh[a,*], Pooya Jafari[b], Babak Farshighazani[a]
Mostafa Keshavarz Moraveji[a]

[a]*Chemical Engineering Department, Amirkabir University of Technology, Tehran, Iran, Tel. +98 715 2872097; emails: mohsenhasanizade@aut.ac.ir (M. Hasanizadeh), farshibabak@yahoo.com (B. Farshighazani), moraveji@aut.ac.ir (M.K. Moraveji)*
[b]*Department of Civil and Environmental Engineering, University of Houston, 4800 Calhoun St., Houston, TX 77204–4003, USA, email: pooyajafari1988@gmail.com*

Received 13 May 2014; Accepted 27 August 2015

ABSTRACT

In this study, direct-contact membrane distillation (DCMD) process is simulated using computational fluid dynamics. The DCMD process is typically used to provide pure water from salt water. The system consists of a flat-sheet membrane, a feed channel with salt water as the food, and a permeate channel. The cross-current flow pattern is used in this process. The governing equations to simulate the process include the heat, mass, and momentum balance equations. The developed equations are solved numerically using the finite element scheme. To improve accuracy of the simulation results and precision of water vapor diffusion coefficient estimation in membrane pores, a composition of Poiseuille and Knudsen diffusion coefficient is applied. The simulation results are compared with experimental data obtained from the literature and a satisfactory agreement is obtained (average error less than 5%).

Keywords: Membrane; Direct-contact membrane distillation (DCMD); Computational fluid dynamics (CFD); Cross-current pattern; Finite element; Poiseuille and Knudsen diffusion coefficient

1. Introduction

Membranes are used to separate azeotropic liquid mixtures or liquids that have very close boiling points. Membranes may be preferred against the other traditional processes such as distillation, which have problems like high operational costs and low selectivity [1]. Membranes are used to remove suspended solids, colloidal materials, bacteria and viruses, dye and mono and divalent ions in food and pharmaceutical industries as well as to produce drinking water in microfiltration, ultrafiltration, nanofiltration, and reverse osmosis processes.

A novel membrane separation process is the membrane distillation (MD) which is capable of the separation of particles as small as 0.1–7 nm. This feature allows the process to be used in a number of applications such as water desalination to provide fresh drinking water and industrial purposes; therefore, the MD has received increasing attention in recent years.

*Corresponding author.

Also, the MD process is used to concentrate juice due to low temperature, keeping color, smell, taste, and vitamins as well as to separate organic and inorganic acids [2].

The reverse osmosis process is used as the main process to produce drinking water [3]. The maximum water purity achieved in reverse osmosis is 98%, whereas in the MD process 100% purity could be achieved. The following advantages are pointed out for MD:

(1) Lower energy requirements in comparison with other similar membrane and conventional distillation processes.
(2) Separation of azeotropic solutions. Banat et al. [4] have reported that by using various inert gasses, the purity of the product obtained from azeotropic feed solution may be increased.
(3) Simplicity and ease of maintenance.
(4) No need of using especial chemicals in food industries.
(5) Low operating costs.

The driving force for MD process is given by the vapor pressure gradient across the membrane which is caused by a temperature difference between the hot and the cold streams on two sides of membrane. The Antoine equation is often used to calculate vapor pressure. In MD process, a hydrophobic porous membrane is used. The hydrophobic nature of membrane prevents the feed liquid solution from penetrating into the membrane pores due to surface tension forces, and only vapor can pass through the membrane. Gas–liquid equilibrium is the basis of the MD process. Hot fluid is evaporated across the feed channel, due to the vapor pressure gradient between the two sides of the membrane caused by temperature difference. The produced vapor passes through pores of the hydrophobic porous membrane and is condensed on the other side of the membrane in contact with cold liquid [5].

The MD process is preferred for small-scale cases where waste energies such as exhaust gas emissions and solar energy could be applied. According to permeate conditions in the MD process, this process can be divided into four kinds:

(1) Direct-contact membrane distillation (DCMD), in which the membrane is direct contact with the hot and the cold fluids. This method is proper for desalination purposes [6].
(2) Air-gap membrane distillation, in which there is a gap between membrane and the condensation surface filled with air. The vapor passed through the gap is condensed in contact with the condensation surface. The air gap limits heat loss between the feed channel and the condensation surface. As a result, the temperature gradient between the feed channel and the condensation surface remains constant over time, and the membrane performance is not disrupted [7].
(3) Sweeping gas membrane distillation, in which an inert gas is used to reduce the boundary layer resistance and thereby the mass flux is increased [8].
(4) Vacuum membrane distillation, in which vacuum is used to enhance the performance of MD. Vacuum reduces diffusion resistance by removing gas trapped in the hole [9].

All the above MD techniques can be used in desalination process. DCMD process has attracted much more attention due to its ease of use and low temperature for condensation of water [10]. To contact between the hot and the cold liquid phases in the DCMD, flat-sheet membranes are typically used. Most of the hydrophobic porous membranes used in DCMD process are polytetrafluoroethylene (PTFE), polypropylene (PP), and polyvinylidene fluoride (PVDF) [11].

Several studies have been conducted to examine the effect of membrane properties on overall mass, momentum, and heat transfer processes. The researches have typically focused on modification of membrane characteristics, whereas few papers have considered the simulation and modeling of transport phenomena, including heat, mass, and momentum transfer in DCMD process.

In order to analyze the transport mechanism in the DCMD process, the process should be modeled and simulated. The transfer phenomena considered in DCMD process involve heat, mass, and momentum transports, so the modeling of this process is mainly difficult. Recently, computational fluid dynamics (CFD) technique is applied by a number of researchers for modeling membrane processes. In this technique, numerical approaches such as finite element method are used to solve the heat, mass, and momentum balance equations. Using CFD, a two-dimensional heat transfer model has been presented for hollow fiber membrane module by Yu et al. [12]. Furthermore, a number of researchers have simulated hollow fiber membrane modules, which are used for gas separation and solvent extraction [13].

The resistance-in-series model is another method that can be used to simulate water desalination process in porous hydrophobic membranes. This method considers key parameters affecting the MD process. In addition, the Monte Carlo simulation model could be

applied to evaluate and describe water flux in DCMD process [14].

This paper aims to simulate the DCMD process for desalinated water production based on CFD technique. The governing equations include the heat, mass, and momentum balance equations which are developed in the following sections.

2. Theory of simulation

In this section, a mathematical model is developed to simulate DCMD process. The model considers transport phenomena including heat, mass, and momentum transports. In the DCMD process, heat and mass transfers occur simultaneously. As the cold and the hot water exist in the membrane modulus, the momentum transfer is included in the model as well. The heat transfer is from the hot side to the cold side and heat transfer within the membrane involves the latent heat needed for evaporation of the water and the heat transferred in the membrane by conduction across both the vapor filled pores and solid membrane material. The major assumptions made in this simulation are as follows:

(1) Steady-state operation.
(2) No chemical reaction occurs.
(3) Laminar flow in both the cold and the hot streams.
(4) The salt rejection is 100%.
(5) Neglected heat loss to the ambient.

In this process, a flat-sheet membrane module is used to connect the hot and the cold stream phases. A cross-flow pattern is considered. Various regions of the membrane module considered to develop the mathematical model are shown schematically in Fig. 1.

As it is shown in Fig. 1, the salty water as the hot feed stream is passed over one side of membrane module, whereas the cold stream is passed from the other side. The process driving force is the temperature difference between the hot and the cold streams. Water evaporates at the feed–membrane interface. The produced vapor passes through membrane pores through diffusion and is condensed on the other side of membrane which is in contact with the cold stream. Due to the hydrophobic nature of the membrane, the produced vapor is passed through which the liquid water cannot pass.

2.1. Governing equations of the model

As it is shown in Fig. 1, the DCMD process consists of three zones including the feed channel, where

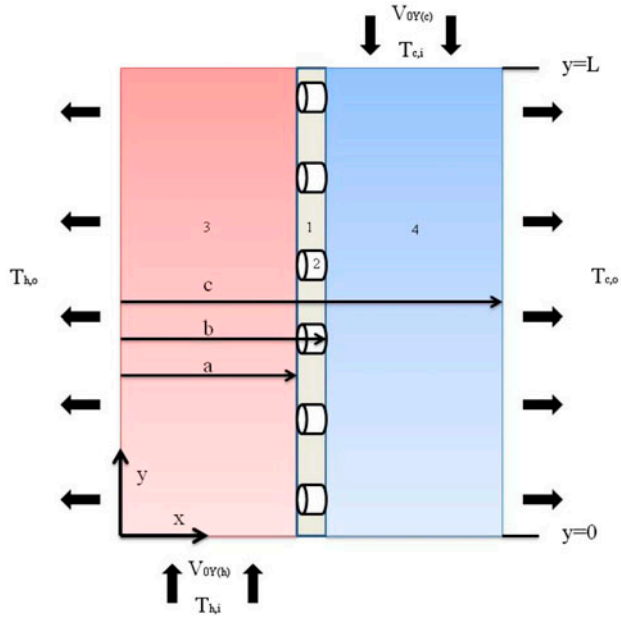

Fig. 1. Various regions considered in the developed model: (1) membrane, (2) pores, (3) feed channel, and (4) permeate channel.

in the hot stream is flowing, the membrane, and the permeate channel, where in the cold stream is flowing. The governing equations should be derived for each of these three zones. In the feed channel, a salty water solution flows. The governing equations in the feed channels include heat, mass, and momentum transfer equations. The heat transfer equation, taking into account the convective and conductive heat transfer mechanisms, is represented as follows [15]:

$$\rho_h C_{ph} V_{Y(h)} \cdot \nabla T_h - \nabla \cdot (k_h \nabla T_h) = 0 \quad (1)$$

or,

$$k_h \left[\frac{\partial^2 T_h}{\partial x^2} + \frac{\partial^2 T_h}{\partial y^2} \right] = \rho_h C_{ph} V_{Y(h)} \frac{\partial T_h}{\partial y} \quad (2)$$

where ρ_h is liquid density, C_{ph} is heat capacity at -constant pressure, k_h is thermal conductivity of liquid, $V_{Y(h)}$ is velocity vector, and T_h is temperature of hot solution.

The mass transfer model in the feed channel containing terms of the convection–diffusion transport of water is represented as follows [16]:

$$D_{w,h} \left[\frac{\partial^2 C_{w,h}}{\partial x^2} + \frac{\partial^2 C_{w,h}}{\partial y^2} \right] = V_{Y(h)} \frac{\partial C_{w,h}}{\partial y} \quad (3)$$

where $D_{w,h}$ is water diffusion coefficient in salty water, $C_{w,h}$ is water concentration in feed channel, and $V_{Y(h)}$ is velocity vector. The Wilke–Chang equation [17] is used for calculating the diffusion coefficient of water in salty water, namely:

$$D_{ij} = \frac{7.4 \times 10^{-8} (\phi M_j)^{1/2} T}{\mu_i v_i^{0.6}} \tag{4}$$

In order to determine temperature and concentration profiles, $V_{Y(h)}$ should be calculated. This parameter is determined using the Navier–Stokes equation. The latter is represented as follows, for the feed channel in the laminar flow conditions [18]:

$$\rho_h \frac{\partial V_{Y(h)}}{\partial t} - \nabla \times \eta(\nabla V_{Y(h)} + (\nabla V_{Y(h)})^{T(h)}) + \rho(V_{Y(h)} \cdot \nabla) V_{Y(h)} + \nabla p = f \tag{5}$$

where η is dynamic viscosity, p is pressure, and f is external force.

The governing equations in the membrane include the heat and mass balance equations. The temperature distribution in membrane pores is obtained through developing the heat balance equation. The conductive heat transfer in membrane is represented using the following equation [19]:

$$\nabla \cdot (K_m \nabla T_m) = 0 \tag{6}$$

or,

$$K_m \left[\frac{\partial^2 T_m}{\partial x^2} + \frac{\partial^2 T_m}{\partial y^2} \right] = 0 \tag{7}$$

where T_m is temperature inside the membrane, and K_m is thermal conductivity of membrane that is calculated from the following relation [11]:

$$K_m = \varepsilon K_g + (1 - \varepsilon) K_s \tag{8}$$

where K_s is thermal conductivity of solid membrane (=0.178) [20] and K_g is that of vapor inside membrane pores. The latter is calculated using the following relation [20]:

$$K_g(T_m) = 0.0144 - 2.16 \times 10^{-5} \ (T_m + 273.15) \tag{9}$$

In the above equation, T_m is mean temperature of membrane, P_1^{sat} and P_2^{sat} are saturated vapor pressure of water at membrane–solution interface and at the hot and cold sides, respectively. Vapor pressure is calculated using Antoine equation represented as follows [20]:

$$P_i^{sat} = 133.322 \times 10^{(8.10765 - (1450.286/(T_i + 235)))} \quad i = 1,\ 2 \tag{10}$$

where T_i is temperature (°C).

The vapor pressure of water is affected by the addition of a non-volatile solute like salt. The effects of non-volatile solutes, such as salt on the vapor pressure of water should be considered to improve the model's results. For non-ideal solutions, partial pressure of water is calculated as using the following relation [20]:

$$P_1^{sat} = y_w P = x_w a_w P_w^{sat} \tag{11}$$

where a_w is activity of water in salty water that is given by:

$$a_w = 1 - 0.5\, x_{NaCl} - 10\, x_{NaCl}^2 \tag{12}$$

To model the water vapor transfer through the membrane, the concentration distribution equation is developed as follows [19]:

$$D_{w,m} \left[\frac{\partial^2 C_{w,m}}{\partial x^2} + \frac{\partial^2 C_{w,m}}{\partial y^2} \right] = 0 \tag{13}$$

where $D_{w,m}$ is diffusion coefficient of water inside membrane pores and $C_{w,m}$ is water concentration. $D_{w,m}$ is determined based on a combination of the Knudsen and the Poiseuille equations as follows [21]:

$$D_{i,m} = \left(\frac{1}{D_K} + \frac{1}{D_P} \right)^{-1} \tag{14}$$

In Eq. (14), D_K is Knudsen diffusivity and D_P is Poiseuille diffusivity which are calculated using the following relations, respectively,

$$D_K = 9.7 \times 10^3 \frac{d_p}{2} \sqrt{\frac{T}{M}} \tag{15}$$

$$D_P = \frac{p \times d_p^2}{16 \times \mu} \tag{16}$$

The governing equations in the permeate channel including the heat, mass, and momentum balance equations

should be derived. The energy balance equation yields an equation representing temperature distribution in the cold solution of the following form [15]:

$$\rho_c C_{pc} V_{Y(c)} \cdot \nabla T_c - \nabla \cdot (k_c \nabla T_c) = 0 \tag{17}$$

or,

$$k_c \left[\frac{\partial^2 T_c}{\partial x^2} + \frac{\partial^2 T_c}{\partial y^2} \right] = \rho_c C_{pc} V_{Y(c)} \frac{\partial T_c}{\partial y} \tag{18}$$

where ρ_c is density of cold liquid, C_{pc} is specific heat at constant pressure, k_c is thermal conductivity of liquid, $V_{Y(c)}$ is velocity vector, and T_c is temperature of cold solution.

Furthermore, the concentration distribution is determined by developing the mass balance equation in the permeate channel, namely [16]:

$$D_{w,c} \left[\frac{\partial^2 C_{w,c}}{\partial x^2} + \frac{\partial^2 C_{w,c}}{\partial y^2} = V_{Y(c)} \frac{\partial C_{w,c}}{\partial y} \right] \tag{19}$$

To solve the above equations, $V_{Y(c)}$, the velocity vector in y direction, is determined based on the Navier–Stokes equation. The latter is represented for the permeate channel as follows [18]:

$$\rho_c \frac{\partial V_{Y(c)}}{\partial t} - \nabla \times \eta (\nabla V_{Y(c)} + (\nabla V_{Y(c)})^{T(c)}) + \rho (V_{Y(c)} \cdot \nabla) V_{Y(c)} + \nabla p = f \tag{20}$$

Table 1
Parameters used in the simulation of DCMD

Parameter	Value	Unit	Refs.
Pore size (μm)	0.22	μm	[22]
Thickness (μm)	178	μm	[22]
Porosity (%)	70	%	[22]
Effective membrane area	0.0169	m^2	[22]
T_{c0} (K)	293.15	K	[22]
T_{h0} (K)	353.15	K	[22]
Q_h	800	ml/min	[22]
Q_c	100, 200, 300, 400	ml/min	[22]
K_h	0.64	W/m/K	[20]
K_c	0.6	W/m/K	[20]
K_m	calculated	W/m/K	[11]
K_s	0.178	W/m/K	[11]
a	0.0003485	m	[22]
b	0.0005265	m	[22]
c	0.000875	m	[22]
L	0.13	m	[22]

Table 2
Boundary condition used for numerical simulation of DCMD

Position	Phenomenon	$x = 0$	$x = a$	$x = b$	$x = c$	$y = 0$	$y = L$
Feed channel	Heat transfer	Convective flux	$T_h = T_m$	–	–	$T_h = T_{0h}$	Thermal insulation
	Mass transfer	Convective flux	$C_{w,h} = C_{w,m} \times m$	–	–	$C_{w,h} = C_0$	No flux
	Momentum transfer	$p = p_{atm}$	No slip	–	–	$V_{Y(h)} = V_{0h}$	No slip
Pores Membrane	Heat transfer	–	$T_m = T_h$	$T_m = T_c$	–	Thermal insulation	Thermal insulation
	Mass transfer	–	$C_{w,m} = C_{w,h}/m$	$C_{w,m} = C_{w,c}$	–	–	–
	Heat transfer	–	–	$T_c = T_m$	Convective flux	Thermal insulation	$T_c = T_{0c}$
Permeate channel	Mass transfer	–	–	$C_{w,c} = C_{w,m}$	Convective flux	No flux	$C_{w,c} = 0$
	Momentum transfer	–	–	No slip	$p = p_{atm}$	No slip	$V_{Y(c)} = V_{0c}$

The parameters used in this simulation are listed in Table 1. The boundary conditions applied for the three zones considered are summarized in Table 2.

3. Numerical solution of governing equations

The governing equations developed in the previous section with the boundary condition are solved using COMSOL software, v3.4 (1,066 MHz CPU speed, 4 GB RAM). The software solved equations based on finite element method. Also, UMFPACK direct solver was used to perform numerical solution. The latter is suitable for numerical solution of non-stiff and stiff non-linear boundary value problems. The performance and accuracy simulating transport phenomena in membrane modules has been confirmed by researchers [23]. The numerical simulation flowchart is shown in Fig. 1. The meshes generated by COMSOL for membrane contactor is shown in Figs. 2. Fig. 3 shows a flowchart of the numerical solution applied. Adaptive mesh refinement in COMSOL, which generates the optimum meshes, was selected to mesh the DCMD module geometry. Due to the large difference between the y and x directions, an index of 100 is used for y-direction. The mesh generated for the process is such that the simulation results are independent of mesh density. Table 3 summarizes the used parameters and details of the mesh generated.

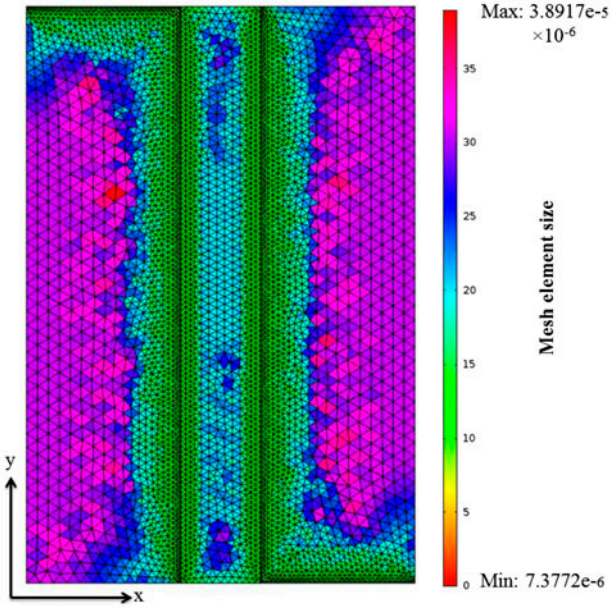

Fig. 2. The mesh generated for simulating the DCMD process.

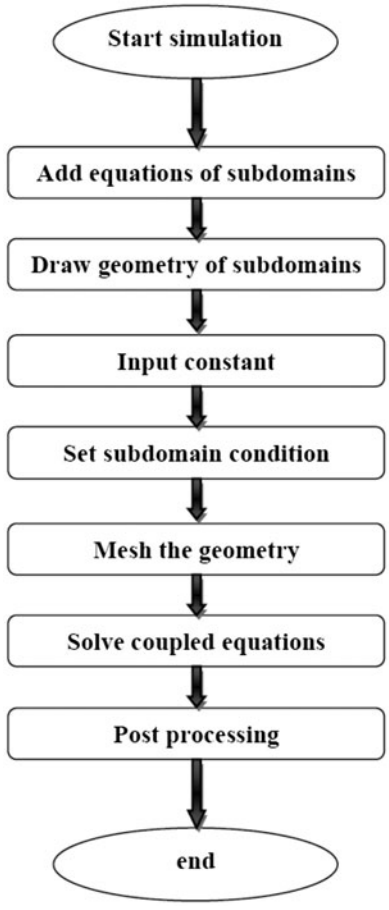

Fig. 3. A flowchart of the numerical optimization method.

4. Results and discussion

4.1. Model's validation

To evaluate the accuracy of the developed model, the simulated results should be validated against experimental data. A comparison between the model's results with the experimental data extracted from the literature is presented in Table 4. As it is seen in this table, a good agreement between experimental data and simulation results is revealed with a maximum error of 7.9% for the cold fluid flow rate of 100 ml/min.

Table 3
The used parameters and details of the mesh generated for the simulation of DCMD process

No. of elements	36,792
No. of degree of freedom	198,080
Mesh shape	Free triangular
Relative tolerance	3.0×10^{-6}
Maximum no. of iterations	8

Table 4
Comparison of the modeling results and the experimental data for water flux in DCMD process

Cold stream flow rate (ml/min)	Flux (L/m^2 h)		
	Modeling	Experimental	Deviation (%)
400	51.02	47.63	7.1
300	47.24	47.33	0.2
200	43.03	44.35	2.9
100	36.29	39.43	7.9

An average error less than 5% indicates the suitability of the model to simulate the operating parameters including inlet velocity and inlet temperature, and design parameters including module geometry of DCMD process [24].

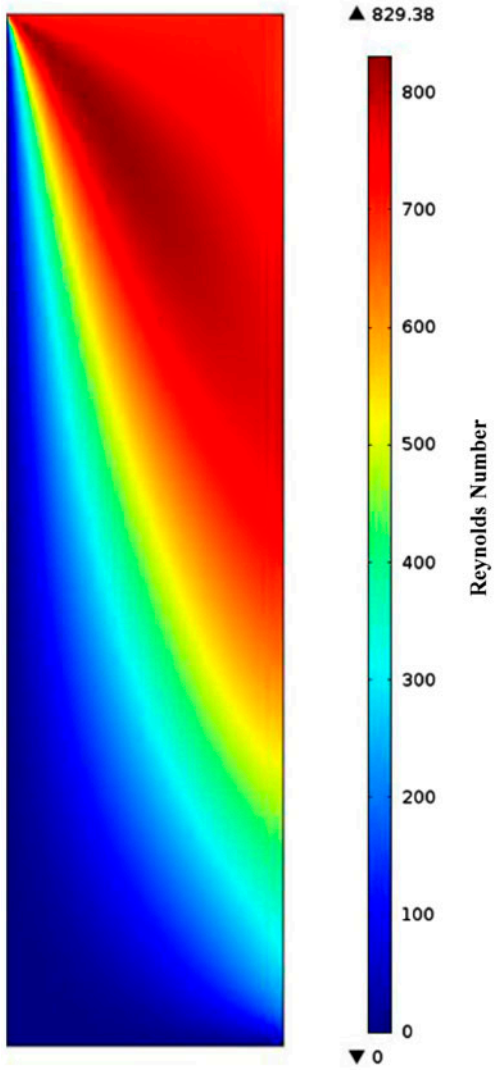

Fig. 4. Reynolds number distribution in the permeate side in DCMD process.

4.2. Hydrodynamics of Process

The hydrodynamic of process with the velocity, pressure, and Reynolds number as its main parameters is very important in the DCMD process. For hydrodynamic modeling, the Navier–Stokes equations are simplified and solved. The latter benefits the consideration of entrance effects in modeling of the velocity distribution profile [25]. Therefore, a Newtonian compressible fluid is assumed and the Reynolds number is calculated. The distribution and profile of Reynolds number in the permeate channel are shown in Figs. 4 and 5, respectively. As it is seen in Fig. 4, at the entrance of the module near the membrane walls, Reynolds number has its maximum value. This maximum increases with the fluid flow rate.

According to Figs. 4 and 5, the Reynolds number at the inlet region has its largest value. In other words, the velocity in the regions near the permeate channel entrance is high, whereas it decreases with increasing y due to approaching to the wall boundary conditions (see Fig. 1). Furthermore, Figs. 4 and 5 confirm the assumption of laminar flow in the membrane module.

Fig. 6 shows the pressure profile along the permeate channel length. Up to the end wall of channel which acts as an obstacle in the path of the fluid (see Fig. 1), the pressure profile exhibits different behaviors; it increases near the entrance, for various flow rates, then decreases and finally increases. According to Fig. 6, the higher the flow rate, the higher the changes in pressure variations along the permeate channel.

4.3. Contours of temperature

Temperature is another important parameter in the analysis of DCMD process. By solving the energy balance equation on the membrane, hot and cold sides of the channel, the temperature profiles can be calculated. The driving force for water transport is the temperature difference between the two sides of the membrane. The temperature contours obtained in permeate channel are shown in Fig. 7.

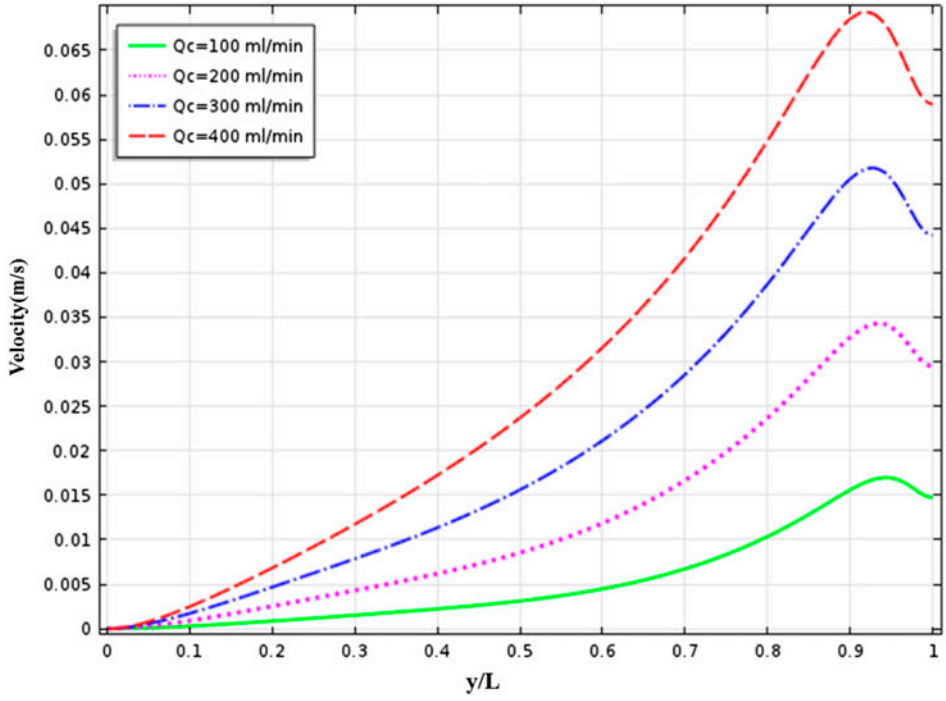

Fig. 5. Profile of Reynolds number in permeate channel.

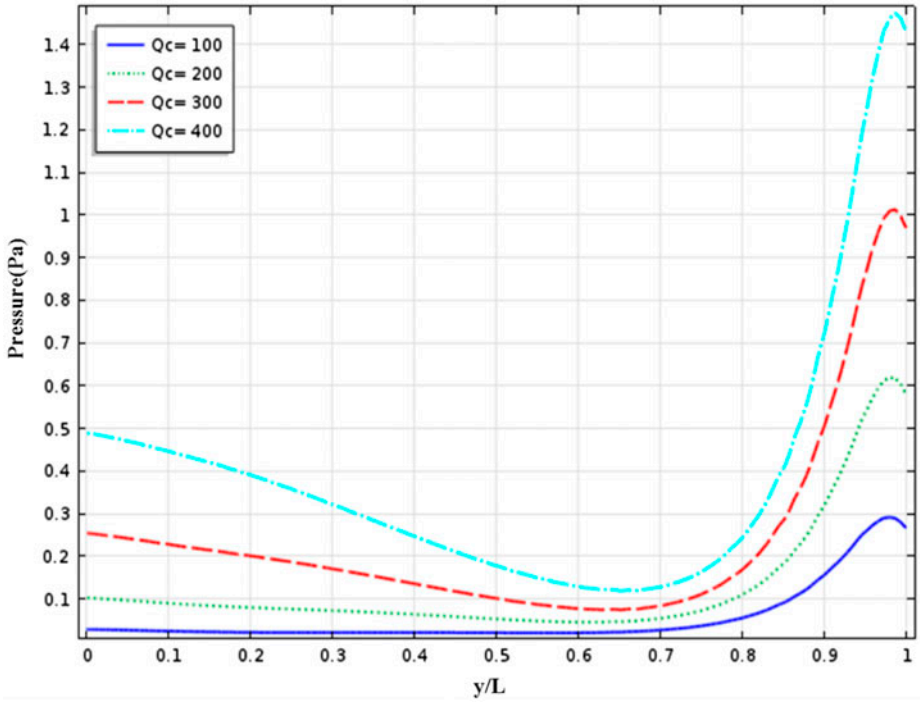

Fig. 6. Profile of pressure for different flow rates in permeate channel.

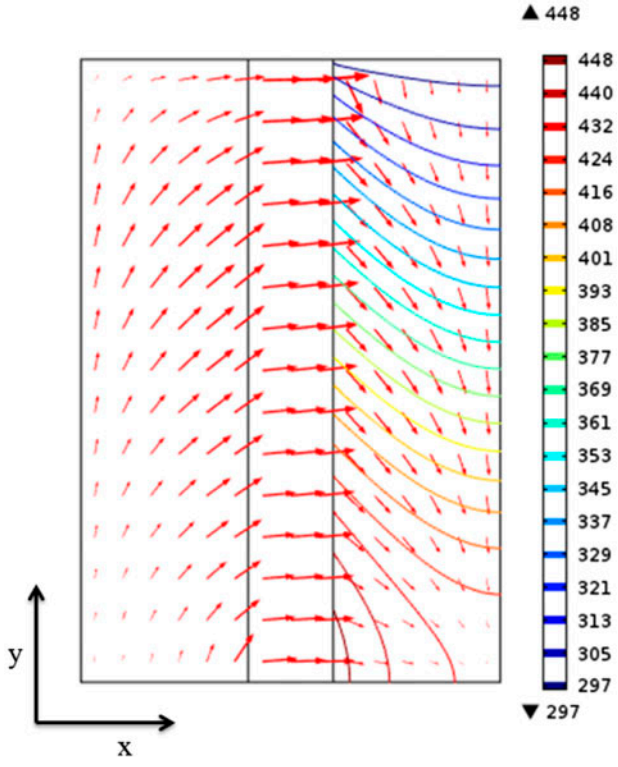

Fig. 7. Temperature contours obtained in the permeate channel.

Cold fluid flows in permeate channel and its temperature increases along the channel due to heat received from the hot fluid. As it is shown in Fig. 7, temperature in permeate channel in regions far from the membrane walls is low and almost constant, while it changes significantly near the membrane walls. It is also observed that temperature difference along the module length is significant in regions adjacent to the membrane wall. This is due to the formation of thermal boundary layer, which is called as temperature polarization. As the arrows in Fig. 7 show, the heat transfer direction is from the hot side to cold side. The heat transfer mechanism in the both feed and permeate channels is convection–conduction and that in the membrane is conduction.

4.4. Temperature profile along the feed channel

To analyze the temperature increase along the permeate channel, the temperature profiles is shown in Fig. 8. The energy required for water to be evaporated from feed channel to permeate channel in the DCMD process is supplied by the hot fluid. Fig. 8 shows the temperature increase along the permeate channel with a remarkable change in regions near the wall which is attributed to the fact that a thermal boundary layer is formed near the membrane wall so

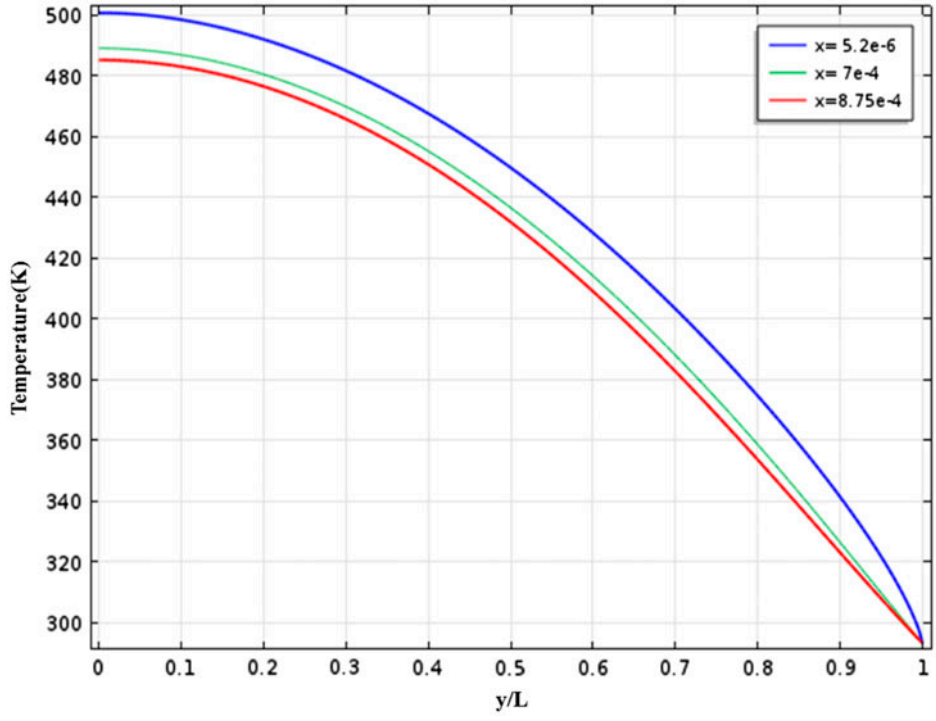

Fig. 8. Profile of temperature in the permeate channel in DCMD process.

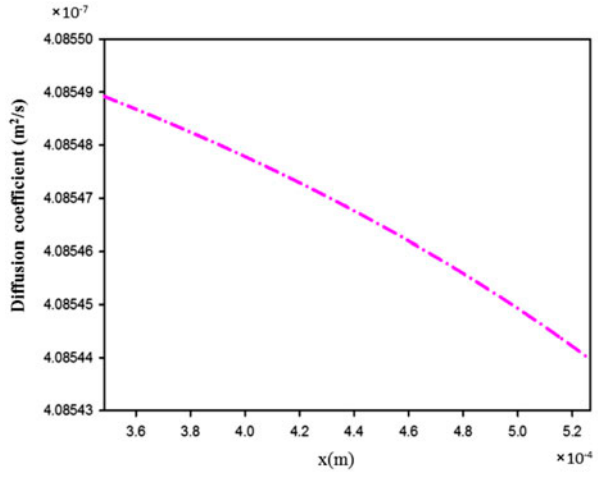

Fig. 9. Profile of diffusion coefficient in membrane pores in DCMD process.

high temperature changes in this region are achieved. This phenomenon is called thermal polarization. Since the saturation pressure depends exponentially on the temperature, hence with reducing the pressure gradient, the water evaporation flux is decreased [6,11,26,27]. Furthermore, a lower temperature changes in the region far from the membrane wall is due to the high contribution of convective heat transfer. In the regions close to the feed channel entrance, a high convective heat transfer occurs which is decreased in *y*-direction due to approaching to the wall boundary conditions. Also, a high portion of convection near the entrance of channel is explained via velocity distribution in feed channel, as the convective heat transfer rate depends on the velocity of solution.

4.5. Profile of diffusive coefficient of mass transfer

The mass transfer of water vapor through membrane pores in the DCMD is very important. The latter is modeled using the continuity equation. In order to increase the accuracy of the model, a combination of Knudsen and Poiseuille diffusion coefficient is applied to calculate the diffusion coefficient of water vapor in the membrane. Fig. 9 illustrates profile of diffusion coefficient of water vapor in membrane pores. In *x*-direction, the diffusivity of water vapor decreases, hence, the water vapor mass transfer in membrane pores is decreased.

5. Conclusions

In this paper, the water desalination by DCMD is simulated using CFD. The simulation is performed in order to determine the distribution of pressure, temperature, diffusion coefficient of water vapor, and Reynolds number in membrane modules. The governing equations of the DCMD process including the heat, mass, and momentum balance equations are solved using finite element method. In order to check the accuracy of the developed model, the simulated results are compared and validated with experimental data and a satisfactory agreement is achieved. According to the simulation results, the cold fluid velocity in the permeate channel near the channel entrance is larger than that in the other regions. The velocity decreases in *y*-direction in the channel due to approaching to the wall conditions, and finally it decreases rapidly to zero. In addition, by cold fluid flowing in the permeate channel, because the temperature increase along the contactor, the pressure gradient of water vapor is increased. The diffusivity of water vapor in the membrane is decreased in *x*-direction, due to the decrease in temperature.

Nomenclatures

C_{pc}	—	cold side specific heat capacity at constant pressure (J/kg K)
C_{ph}	—	hot side specific heat capacity at constant pressure (J/kg K)
C_{pm}	—	specific heat capacity of the membrane at constant pressure (J/kg K)
k	—	thermal conductivity (W/m K)
k_c	—	cold side liquid thermal conductivity (W/m K)
k_h	—	hot side liquid thermal conductivity (W/m K)
K_m	—	liquid thermal conductivity of the membrane (W/m K)
L	—	module length (m)
m	—	partial coefficient
p	—	pressure (Pa)
p_c	—	cold side pressure (Pa)
p_h	—	hot side pressure (Pa)
T_c	—	cold side temperature (K)
T_{0c}	—	cold side inlet temperature (K)
T_h	—	hot side temperature (K)
T_{0h}	—	hot side inlet temperature (K)
T_m	—	membrane temperature (K)
$V_{c(Y)}$	—	cold side flow velocity (m/s)
$V_{h(Y)}$	—	hot side flow velocity (m/s)
V_{0c}	—	cold side inlet flow velocity in vertical direction (m/s)
V_{0h}	—	hot side inlet flow velocity in vertical direction (m/s)
X	—	*x*-direction
Y	—	*y*-direction

$D_{w,h}$ — diffusion coefficient of water in salty water (m^2/s)
$D_{w,m}$ — diffusion coefficient of water in membrane (m^2/s)
$D_{w,c}$ — diffusion coefficient of water in permeate (m^2/s)
D_P — Poiseuille diffusion coefficients (m^2/s)
D_K — Knudsen diffusion coefficients (m^2/s)

Greek letter

v — molar volume (cm^3/mol)
μ — viscosity (cp)
ρ — density (kg/m^3)
ε — membrane porosity

References

[1] M. Khayet, T. Matsuura, Membrane Distillation: Principles and Applications, Elsevier, kidlington, 2011.
[2] T. Mohammadi, M. Akbarabadi, Separation of ethylene glycol solution by vacuum membrane distillation (VMD), Desalination 181 (2005) 35–41.
[3] M. Izquierdo-Gil, C. Fernández-Pineda, M. Lorenz, Flow rate influence on direct contact membrane distillation experiments: Different empirical correlations for Nusselt number, J. Membr. Sci. 321 (2008) 356–363.
[4] F.A. Banat, F. Abu Al-Rub, R. Jumah, M. Shannag, On the effect of inert gases in breaking the formic acid–water azeotrope by gas-gap membrane distillation, Chem. Eng. J. 73 (1999) 37–42.
[5] M. Khayet, Membranes and theoretical modeling of membrane distillation: A review, Adv. Colloid Interface Sci. 164 (2011) 56–88.
[6] A. Imdakm, T. Matsuura, Simulation of heat and mass transfer in direct contact membrane distillation (MD): The effect of membrane physical properties, J. Membr. Sci. 262 (2005) 117–128.
[7] E. Guillén-Burrieza, G. Zaragoza, S. Miralles-Cuevas, J. Blanco, Experimental evaluation of two pilot-scale membrane distillation modules used for solar desalination, J. Membr. Sci. 409–410 (2012) 264–275.
[8] M. Khayet, M. Godino, J. Mengual, Theoretical and experimental studies on desalination using the sweeping gas membrane distillation method, Desalination 157 (2003) 297–305.
[9] K.W. Lawson, D.R. Lloyd, Membrane distillation. II. Direct contact MD, J. Membr. Sci. 120 (1996) 123–133.
[10] A. Alklaibi, N. Lior, Membrane-distillation desalination: Status and potential, Desalination 171 (2005) 111–131.
[11] H.J. Hwang, K. He, S. Gray, J. Zhang, I.S. Moon, Direct contact membrane distillation (DCMD): Experimental study on the commercial PTFE membrane and modeling, J. Membr. Sci. 371 (2011) 90–98.
[12] H. Yu, X. Yang, R. Wang, A.G. Fane, Analysis of heat and mass transfer by CFD for performance enhancement in direct contact membrane distillation, J. Membr. Sci. 405–406 (2012) 38–47.
[13] S. Shirazian, S.N. Ashrafizadeh, 3D modeling and simulation of mass transfer in vapor transport through porous membranes, Chem. Eng. Technol. 36 (2013) 177–185.
[14] M. Qtaishat, T. Matsuura, B. Kruczek, M. Khayet, Heat and mass transfer analysis in direct contact membrane distillation, Desalination 219 (2008) 272–292.
[15] J. Phattaranawik, R. Jiraratananon, Direct contact membrane distillation: Effect of mass transfer on heat transfer, J. Membr. Sci. 188 (2001) 137–143.
[16] T.-C. Chen, C.-D. Ho, H.-M. Yeh, Theoretical modeling and experimental analysis of direct contact membrane distillation, J. Membr. Sci. 330 (2009) 279–287.
[17] M. Rezakazemi, Z. Niazi, M. Mirfendereski, S. Shirazian, T. Mohammadi, A. Pak, CFD simulation of natural gas sweetening in a gas–liquid hollow-fiber membrane contactor, Chem. Eng. J. 168 (2011) 1217–1226.
[18] J.M. Smith, H.C. Van Ness, M.M. Abbott, Introduction to Chemical Engineering Thermodynamics, McGraw-Hill, Boston, MA, 2005.
[19] S. Shirazian, A. Moghadassi, S. Moradi, Numerical simulation of mass transfer in gas–liquid hollow fiber membrane contactors for laminar flow conditions, Simul. Model. Pract. Theor. 17 (2009) 708–718.
[20] R. Schofield, A. Fane, C. Fell, Heat and mass transfer in membrane distillation, J. Membr. Sci. 33 (1987) 299–313.
[21] H. Chiang, P. Chiang, Y. Chiang, E. Chang, Diffusivity of microporous carbon for benzene and methyl-ethyl ketone adsorption, Chemosphere 38 (1999) 2733–2746.
[22] M.M.A. Shirazi, A. Kargari, M.J.A. Shirazi, Direct contact membrane distillation for seawater desalination, Desalin. Water Treat. 49 (2012) 368–375.
[23] S. Shirazian, M. Rezakazemi, A. Marjani, S. Moradi, Hydrodynamics and mass transfer simulation of wastewater treatment in membrane reactors, Desalination 286 (2012) 290–295.
[24] M. Ghadiri, S. Fakhri, S. Shirazian, Modeling and CFD simulation of water desalination using nanoporous membrane contactors, Ind. Eng. Chem. Res. 52 (2013) 3490–3498.
[25] M. Ghadiri, A. Marjani, S. Shirazian, Mathematical modeling and simulation of CO_2 stripping from monoethanolamine solution using nano porous membrane contactors, Int. J. Greenhouse Gas Control 13 (2013) 1–8.
[26] T.Y. Cath, V.D. Adams, A.E. Childress, Experimental study of desalination using direct contact membrane distillation: A new approach to flux enhancement, J. Membr. Sci. 228 (2004) 5–16.
[27] L. Martínez, J. Rodríguez-Maroto, On transport resistances in direct contact membrane distillation, J. Membr. Sci. 295 (2007) 28–39.